A98-37250

AIAA-98-4343

DESIGN, PERFORMANCE AND MODELING CONSIDERATIONS FOR CLOSE FORMATION FLIGHT

William Blake* and Dieter Multhopp**
Air Force Research Laboratory, Wright Patterson AFB, Ohio

NOMENCLATURE

b	Wing span
AR	Wing aspect ratio
C_{Di}	Induced drag coefficient
C_{Do}	Parasite drag coefficient
C_L	Lift coefficient
C_l	Rolling moment coefficient
C_n	Yawing moment coefficient
η	Non-dimensional lateral spacing between wings, $\Delta y/b$
ζ	Non-dimensional vertical spacing between wings, $\Delta z/b$
ξ	Non-dimensional axial spacing between wings, $\Delta x/b$
μ	Non-dimensional vortex core radius, r/b
σ_{jk}	Influence factor for induced drag
σ_i	$(\sigma_{jk}+\sigma_{jk})/2$ with i=|j-k|
τ_{jk}	Influence factor for induced moments

INTRODUCTION

Advances in automatic control theory in conjunction with increased ability to accurately determine the precise location of aircraft open the possibility of achieving significant increases in range using close formation flight. Properly positioned, each aircraft could fly in the upwash field generated by neighboring aircraft, effectively rotating the lift vector forward, reducing induced drag. It has been conjectured that this drag reduction is one of the reasons that many migratory bird species fly in closely spaced flocks [1]. Detailed photographic measurements of Canadian Geese have found that the average lateral spacing between adjacent birds is very close to the optimum predicted by simple aerodynamic theory [2].

* Aerospace engineer, Associate Fellow AIAA
** Technical area leader, Member AIAA

Most calculations of formation flight benefits are based on a single horseshoe vortex representation of the wing [1,3-6]. Maskew [7] performed extensive calculation using a vortex lattice representation, and used a trim procedure which held lift constant with zero roll. Hummel has used both representations [4] and conducted limited iterative wake roll-up calculations[8]. He also conducted two flight tests in an attempt to demonstrate a power saving under realistic conditions. In his second test, a Dornier-228 acted as a vortex generator for a following Dornier-28. Using an automatic control system to maintain proper position, an average power reduction of 10% was measured on the trail aircraft over a 150 sec. interval.

This paper will explore aspects of the problem not considered by prior investigators. Simplifications including constant specific fuel consumption and uniform aircraft weight across the formation will be relaxed. Optimum flight conditions for a formation will be developed. The effect of accuracy in maintaining lateral position and the effect of rotation of lead aircraft will also be studied. Aerodynamic modeling will be done using the horseshoe vortex and vortex lattice methods. New horseshoe vortex results will be presented using a velocity profile which includes a viscous core.

Throughout this paper, the term "V formation" will be taken to be that used by birds, with the apex of the V in the direction of flight.

DISCUSSION

The total induced drag of a formation of aircraft can be written in matrix form as:

$$C_{Di} = \begin{bmatrix} C_{L,1} & C_{L,2} & \dots & C_{L,j} \end{bmatrix} [G] \begin{bmatrix} C_{L,1} \\ C_{L,2} \\ \dots \\ C_{L,j} \end{bmatrix} \qquad (1)$$

where G is a symmetric matrix given as:

$$[G]=\frac{1}{\pi AR}\begin{bmatrix} 1 & \sigma_1 & \sigma_2 & \cdots & \sigma_j \\ \sigma_1 & 1 & \sigma_1 & \cdots & \sigma_{j-1} \\ \sigma_2 & \sigma_1 & 1 & \cdots & \cdots \\ \cdots & \cdots & \cdots & \cdots & \sigma_1 \\ \sigma_j & \sigma_{j-1} & \cdots & \sigma_1 & 1 \end{bmatrix} \quad (2)$$

The terms in the G matrix are written in Prandtl's [9] compact notation $\sigma_i = (\sigma_{jk}+\sigma_{kj})/2$ where i=|j-k|. The mutual induced drag between a given pair of aircraft is given by the term σ_i. The isolated effect of aircraft j on aircraft k is given by the term σ_{jk} and vice versa. These terms are a function of the relative spacing of the aircraft only. For a single aircraft with an elliptic lift distribution, the self induced drag factor σ_{11} is unity. For a given vertical and lateral spacing of aircraft, the mutual induced drag between any pair of aircraft $\sigma_{jk}+\sigma_{jk}$ is independent of longitudinal spacing, although the individual values vary. This is Munk's stagger theorem [9]. Written in this fashion, the total induced drag of a two aircraft system becomes:

$$C_{Di}=\frac{C_{L,1}{}^2}{\pi AR}+\frac{C_{L,2}{}^2}{\pi AR}+\frac{2C_{L,1}C_{L,2}\sigma_1}{\pi AR} \quad (3)$$

Identical wings, physically joined have an aspect ratio double of the individual wings, giving σ_i=-0.5.

DETERMINATION OF σ

A variety of aerodynamic methods can be used to compute the wake induced forces and moments. The horseshoe vortex model [see Appendix] gives the off diagonal terms in the G matrix as:

$$\sigma_i=\frac{1}{\pi^2}\ln\left[\frac{\zeta^4+2\zeta^2\left(\eta^2+(\frac{\pi}{4})^2\right)+\left(\eta^2-(\frac{\pi}{4})^2\right)^2}{\left(\zeta^2+\eta^2\right)^2}\right] \quad (4)$$

The spacing variables in eq. (4) are shown schematically in Figure 1. Eq. (4) is shown graphically in contour form in Figure 2. Positive values indicate a drag increase, and are evident when the wings overlap to a great extent. Negative values indicate a drag reduction. The size of the beneficial drag region decreases as vertical spacing increases. The "sweet spot" of maximum drag reduction is very small, with a radius the order smaller than a tenth of a wing span.

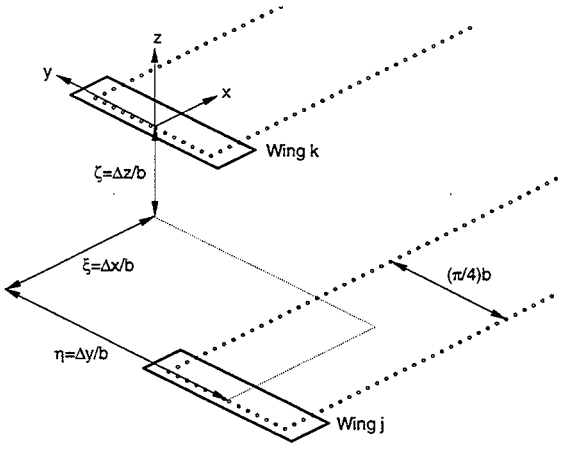

Figure 1. Formation Flight Geometry.

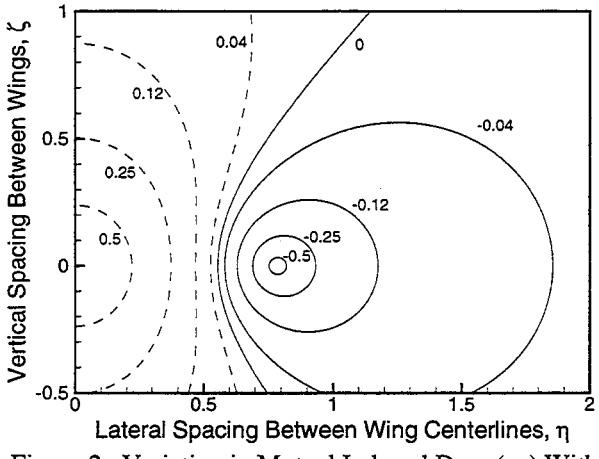

Figure 2. Variation in Mutual Induced Drag (σ_1) With Aircraft Position, Horseshoe Vortex Model.

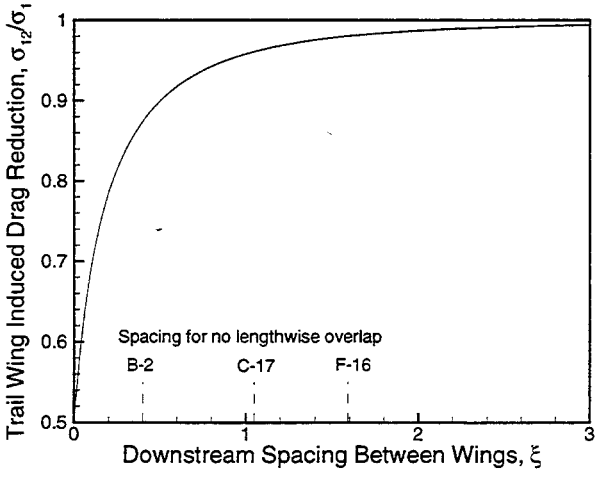

Figure 3. Fraction of Mutual Induced Drag Attained on Downstream Trail Wing, Horsehoe Vortex Model.

The effect of spacing in the downstream direction is shown in Figure 2. This figure shows what fraction of the total drag benefit is received by the trail wing. Also shown on this figure are the lengths of three USAF aircraft , non-dimensionalized by span. A reasonable operational safety requirement is to disallow any lengthwise overlap between aircraft, i.e. require the nose of all aircraft to be behind the tail of the aircraft upstream. This would allow all aircraft freedom of movement in the spanwise direction without possibility of collision. Fig. 2 shows that this means at least two wing spans of downstream separation are required for conventional aircraft. The all wing B-2 configuration is a unique case. At this spacing, 98.5 percent of the benefit is realized at the trail aircraft. For preliminary analyses then , it is reasonable to assume that all of the drag benefit is accrued on trail aircraft.

Eq. (4) result is singular for co-planar (ζ=0) wings if the trailing vortices overlap (η=0, $\pm\pi/4$). Kshatriya and Blake [5] represent this situation in an idealized form by assuming that the overlapping vortices cancel at the trail wing, leaving one tip vortex from each wing. This is equivalent to modeling a physically joined wing. Singularities can also be avoided by using a vortex velocity profile that includes a viscous core. The Rankine "solid body" profile is simple and easily integrated but yields multiple solutions depending on the size and relative orientation of the core and trailing wing tip. The Burnham-Hallock profile [10] has been shown to correlate well with experimental data, is easily integrated, and yields a single solution (see Appendix). The result obtained is similar in form to eq. (4):

$$\sigma_i = \frac{1}{\pi^2}\ln\left[\frac{\zeta^2+\mu^2+(\eta-\pi/4)^2}{\zeta^2+\mu^2+\eta^2}\right] + \frac{1}{\pi^2}\ln\left[\frac{\zeta^2+\mu^2+(\eta+\pi/4)^2}{\zeta^2+\mu^2+\eta^2}\right] \quad (5)$$

Here, μ is the core radius, non-dimensionalized by wing span.

Mutual induced drag can also be calculated using vortex lattice or higher order codes. Results from the vortex lattice code HASC95 [11] are compared with the horseshoe vortex model in Fig. 4. These two methods represent the limiting cases in terms of approach. The horseshoe model assumes a single, fully rolled up vortex while the lattice model includes no roll-up. The HASC95 results are for two untapered aspect ratio eight wings, one span apart in downstream distance. Each wing was represented by 40 evenly spaced spanwise and 5 cosine spaced chordwise elements. The maximum drag reduction from the vortex lattice method occurs at about 5% span overlap, compared to the 22% span overlap for the horseshoe vortex method. The sharp change in the vortex lattice result at the wing tip is inherent in the method [7]. A core radius of 3% span has very little effect for most spacings and approximates the maximum reduction of σ_1=-0.5 for physically joined wings.

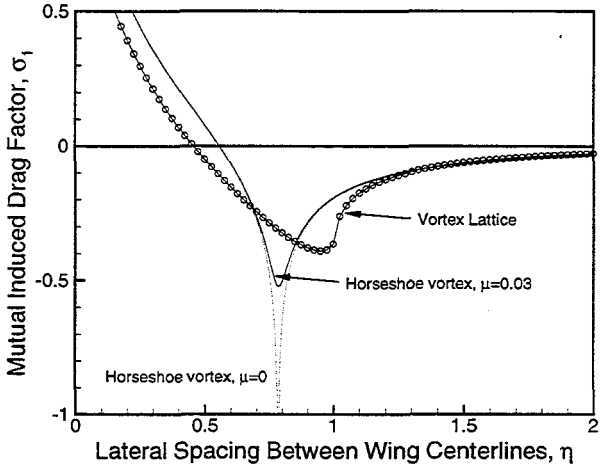

Figure 4. Mutual Induced Drag (σ_1) Predicted by Various Methods, ζ=0.

LIFT DISTRIBUTION FOR MINIMUM DRAG

With total formation lift held constant, the distribution of lift across the formation which minimizes total induced drag is found by differentiating eq. (2) in conjunction with Lagrange multipliers. The result obtained is:

$$\begin{bmatrix} C_{L,1} \\ C_{L,2} \\ \cdots \\ C_{L,j} \end{bmatrix} = \left(\frac{\lambda}{2}\right)[G]^{-1}\begin{bmatrix} 1 \\ 1 \\ \cdots\cdots \\ 1 \end{bmatrix} \quad (6)$$

For a two aircraft formation, equal lift ($C_{L,1} = C_{L,2}$) is the minimum drag solution. This is the biplane result and is one reason that negative relative incidence or *decalage* is used on the forward wing of a staggered biplane.

For a three aircraft formation, minimum induced drag is obtained when $C_{L,1} = C_{L,3}$ and:

$$\frac{C_{L,2}}{C_{L,1}} = 1 + \frac{\sigma_1 - \sigma_2}{\sigma_1 - 1} \tag{7}$$

Eq. (7) is Prantdl's result [9] for the minimum drag loading on a triplane with wings of equal size. In that case, where adjacent wings are in each others downwash, the interference is adverse and the center wing surface should carry less than 1/3 the total lift. In the formation flight case, where interference is favorable, the center wing should carry greater lift than its neighbors. Note that eq. (7) is independent of the formation orientation in the direction of flight. This means that the center wing should be heavier whether it is in the front of a V, the back of a reverse V, or the middle of an echelon. For a four aircraft formation, $C_{L,1} = C_{L,4}$, $C_{L,2} = C_{L,3}$ and:

$$\frac{C_{L,2}}{C_{L,1}} = 1 + \frac{\sigma_1 - \sigma_3}{\sigma_2 - 1} \tag{8}$$

For five aircraft, $C_{L,1} = C_{L,5}$, $C_{L,2} = C_{L,4}$ and:

$$\frac{C_{L,2}}{C_{L,1}} = 1 + \frac{(\sigma_1 - \sigma_4)(\sigma_1 - 1) + (\sigma_2 - \sigma_3)(\sigma_1 - \sigma_2)}{(\sigma_1 - 1)(\sigma_3 - 1) - (\sigma_1 - \sigma_2)^2} \tag{9}$$

$$\frac{C_{L,3}}{C_{L,1}} = 1 + \frac{\sigma_2(\sigma_4 - 1) - \sigma_3(\sigma_1 - 1)}{(\sigma_1 - 1)(\sigma_3 - 1) - (\sigma_1 - \sigma_2)^2} + \frac{(\sigma_1 - \sigma_4)(2\sigma_1 - 1) - (\sigma_3 - \sigma_2)^2}{(\sigma_1 - 1)(\sigma_3 - 1) - (\sigma_1 - \sigma_2)^2}$$

In all cases, the optimum lift distribution is such that the wings at the end of the formation carry the least lift and the wings in the center carry the most.

The presence of one aircraft within a vortex generated by another will alter the vortex. This means that aircraft further downstream will not "see" the same vortex, invalidating the superposition principle inherent in eq. (6). Stewart [12] has investigated the vortex-trail aircraft interaction from the perspective of modeling a wake vortex encounter. By applying conservation of angular momentum to the vortex-trail aircraft system, he treated the effect as an increase in the vortex core radius as the trail aircraft encounters it. For equal airplanes at his nominal condition, Stewart found a 20 percent reduction in roll angle attained after one second when this effect was included. For the present analysis, this effect can be bounded by assuming that 100% of the vortex momentum is removed by the first encountering aircraft. With this assumption, the optimum lift distribution for three aircraft is:

$$\frac{C_{L,2}}{C_{L,1}} = 1 + \frac{\sigma_1}{\sigma_1 - 1} \tag{10}$$

For four aircraft:

$$\frac{C_{L,2}}{C_{L,1}} = 1 - \sigma_1 \tag{11}$$

For five aircraft:

$$\frac{C_{L,2}}{C_{L,1}} = \frac{\sigma_1}{\sigma_1^2 + \sigma_1 - 1} \tag{12}$$

$$\frac{C_{L,3}}{C_{L,1}} = \frac{\sigma_1(1 - \sigma_1)}{\sigma_1^2 + \sigma_1 - 1} \tag{13}$$

A plot of the lift variation for two, five and twelve aircraft formations is shown in Fig. 5. Values of σ were obtained from eq.(6) assuming co-planar wings (ξ=0) with spacing between adjacent wings of 0.85. At this spacing, the effect of the vortex core is small, and the vortex lattice result closely matches the horseshoe model.

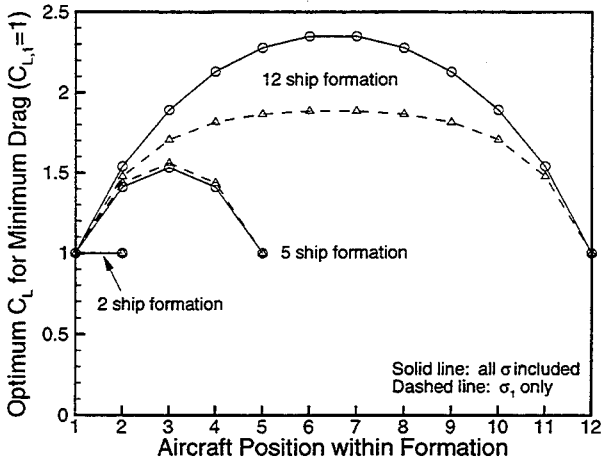

Figure 5. Distribution of Lift Within Formation for Minimum Induced Drag, η=0.85, ζ=0.

Fig. 5 shows that total drag is minimized with an elliptical distribution of aircraft weight across the formation. The effect of ignoring the effect of vortices on non-neighboring aircraft only changes the result for the largest formation, where the optimum distribution is somewhat flatter. For large formations, the optimum lift distributions will not typically be attainable. However, the results can be used as a guide in determining an optimum formation layout and strategy for rotating lead aircraft within a formation.

OPTIMUM FLIGHT CONDITION

The specific range (distance flown per unit fuel expended) of an aircraft formation can be written as:

$$S.R. \equiv \frac{V}{F} = \frac{V}{\sum c_{T,i} T_i} \tag{14}$$

This is often analyzed by assuming constant fuel consumption (c_T) with flight at a specified altitude or speed. For a formation of aircraft, maximizing specific range results in flight at higher C_L relative to a single aircraft. This can be achieved by flying at a higher altitude or slower speed. In either case, the total drag and resultant power setting of aircraft within the formation can be so small that variations in c_T must be considered. Two cases will be examined, constant Mach cruise and constant altitude cruise.

Constant Mach Number

For a constant Mach cruise, with the level flight substitutions T=D and L=W, eq. (14) can be written as:

$$S.R. = \frac{a_o \sqrt{\theta} M}{W_1} \frac{C_{L,1}}{\sum c_{T,i} C_{D,i}} \tag{15}$$

The lift coefficient for maximum specific range can be computed using eqs. (1) and (15). For a two-aircraft formation, the result is:

$$C_{L,1} = \sqrt{\frac{\pi A R C_{Do} \left(1 + \frac{c_{T,2}}{c_{T,1}}\right)}{1 + \frac{C_{L,2}}{C_{L,1}} \left[\left(\frac{C_{L,2}}{C_{L,1}} + \sigma_{12} \right) \frac{c_{T,2}}{c_{T,1}} + \sigma_{21} \right]}} \tag{16}$$

$$C_{L,2} = C_{L,1} (C_{L,2} / C_{L,1})$$

For larger formation sizes, the result is given in matrix form. If c_T increases with reduced power setting, the typical result, eq. (16) indicates that the optimum lift coefficient is larger than if c_T is assumed constant.

Constant Altitude Cruise

For a constant altitude cruise, eq. (14) becomes:

$$S.R. = \sqrt{\frac{2}{\rho S W_1}} \frac{\sqrt{C_{L,1}}}{\sum c_{T,i} C_{D,i}} \tag{17}$$

The relationship for optimum lift with constant Mach and constant altitude cruises for a single aircraft is also obtained for the formation:

$$C_{L,1}\big|_{alt=const} = C_{L,1}\big|_{M=const} / \sqrt{3}$$
$$C_{L,2}\big|_{alt=const} = C_{L,2}\big|_{M=const} / \sqrt{3} \tag{18}$$

Application of the foregoing relationships may result in one of the following results: the thrust required for the lead aircraft exceeds the thrust available, or the thrust required for one of the following aircraft is less than the minimum available (idle). These will require either a change in altitude or speed.

Maximum Relative Range

Relative range is defined as the ratio of the range of a formation relative to a single aircraft [7]. From an aerodynamic perspective, relative range is obtained from the lift-to-drag ratio. Maximum induced drag reduction corresponds to the case of an equivalent joined wing. In this case, the effective aspect ratio of each aircraft in an n aircraft formation is n times the aspect ratio of a single aircraft. If the formation flies at maximum L/D (total induced drag = total parasite drag), the maximum relative range is:

$$\left.\frac{R_{form}}{R_{single}}\right|_{aero} = \sqrt{n} \tag{19}$$

If the formation is constrained to fly at the maximum L/D point of a single aircraft, maximum relative range is greatly reduced, becoming:

$$\left.\frac{R_{form}}{R_{single}}\right|_{aero} = \frac{2n}{n+1} \tag{20}$$

With this constraint, an infinite formation can only double the range of a single aircraft.

From a propulsion system perspective, relative range can be defined as the ratio of the fuel flow of a set of n aircraft in single flight to the same set in formation flight (assuming velocity is the same). The minimum possible fuel flow in formation flight is taken to be all trail aircraft at idle power with the lead aircraft cruise power. Maximum relative range in this case now becomes:

$$\left.\frac{R_{form}}{R_{single}}\right|_{prop} = \frac{n}{1 + (n-1)\frac{FF_{idle}}{FF_{cruise}}} \tag{21}$$

The fuel flow ratio for low bypass turbofans can be as high as one third at cruise altitude.

Preferred Formation Geometry

A symmetrical V formation results in light aircraft in the center and heavy aircraft on the ends, which is the least optimal from a lift distribution viewpoint. A reverse V formation is better, with the heavy aircraft in the middle and light ones on the ends. However, this

formation has a lower relative range (propulsion limited) due to two aircraft instead of one at the cruise fuel flow condition. An echelon formation has successively increasing aircraft weight further from the lead. However, if the lead aircraft rotates to the rear position on a periodic basis, an elliptic weight distribution can be simulated (Fig 6). An echelon geometry also allows freedom of movement in the spanwise direction without possibility of collision. This is a distinct safety feature that both the V and reverse V lack.

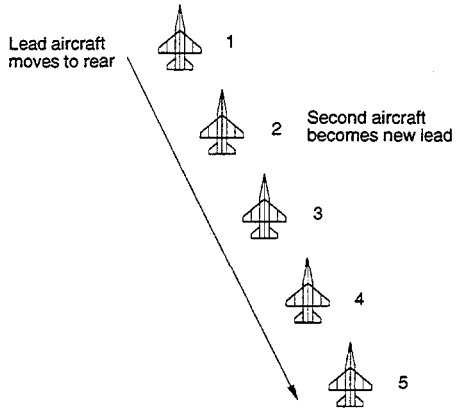

Figure 6. Echelon Formation Geometry.

The so-called "equal power" formation has received considerable attention [1,4]. This formation is designed to have equal drag benefit on all aircraft. Two drawbacks to this formation are that significant lengthwise overlap is required, a safety hazard, and that the lateral spacing is nowhere near optimal, meaning that the drag equality is achieved by having trail aircraft fly in suboptimal position.

NUMERICAL EXAMPLE

This section will examine the effect of formation size, lateral position accuracy and rotation of lead aircraft on relative range. No trim is included. A parabolic drag polar is assumed and the effects of compressibility on both drag and engine performance are ignored. The formation geometry and lead aircraft rotation used are shown in Fig. 6. The analysis is run until one aircraft runs out of fuel, at which point the range calculation stops. A constant Mach cruise (M=0.85) is assumed with aircraft increasing altitude as fuel is burned, subject to a thrust available constraint. Eq. (5) was used to generate values of σ using μ=0.33.

The study vehicle is a lightweight fighter with the following characteristics:

Wing area	300 sq ft
Aspect Ratio	3
Gross Weight	25000 lb
Fuel Weight	7000 lb
C_{do}	0.020

Engine characteristics (thrust and fuel flow as a function of Mach and altitude for various power settings) were taken from the F-16D VISTA simulation developed by McKeehen [13].

Lateral Position

The effect of accuracy in maintaining lateral position on relative range is shown in Fig. 7. Three formation sizes are shown, with a maximum relative range of about 2 attained for the 12 aircraft formation. For this calculation, the aircraft lead was assumed to rotate every ten minutes. Lateral position was varied about the optimum point ($\eta = \pi/4$) by integrating eq. (5) with various lateral intervals and computing the effective σ. About 50% of the maximum achievable benefit is lost if the lateral position cannot be maintained to better than 0.1 span. For an F-16, this translates to +/- 3 feet of position accuracy. As the position error increases, decreases in relative range result as the trail aircraft pass within the high downwash region for extended periods.

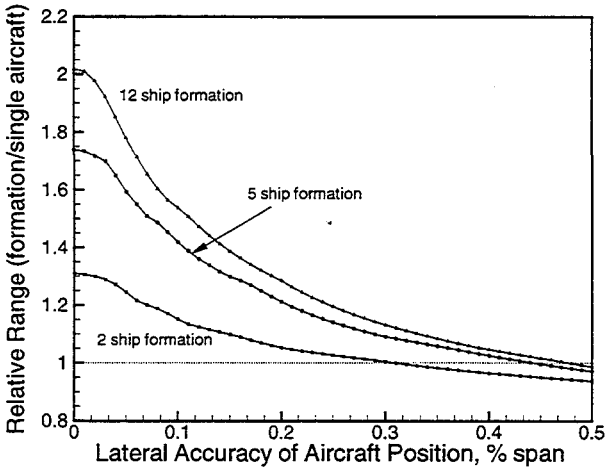

Figure 7. Effect of Lateral Position Accuracy Size on Relative Range. (M=0.85, 10 min rotation)

Ability to maintain a lateral spacing in terms of percent span will not scale with aircraft size. For a given wing

loading and aspect ratio, lateral control power is proportional to the cube of wing span while roll inertia is proportional to the fourth power of span. This means that available angular acceleration will decrease with span.

Rotation of Lead Aircraft

The effect of frequency of lead aircraft rotation on relative range is shown in Fig. 8. Three formation sizes are again shown, with lateral position assumed to be maintained within 0.05 span. Peaks correspond to conditions where all aircraft were low on fuel when the first ran out, conversely, valleys correspond to conditions where some aircraft had a substantial fuel load remaining when the first ran out. The final peak represents the case where each aircraft was in the lead position one time. The desired rotation frequency is proportional to the number of aircraft within the formation. A preferred operating condition may be to rotate position just often enough to avoid the large valleys. For the five aircraft formation, this corresponds to about a 30 minute interval.

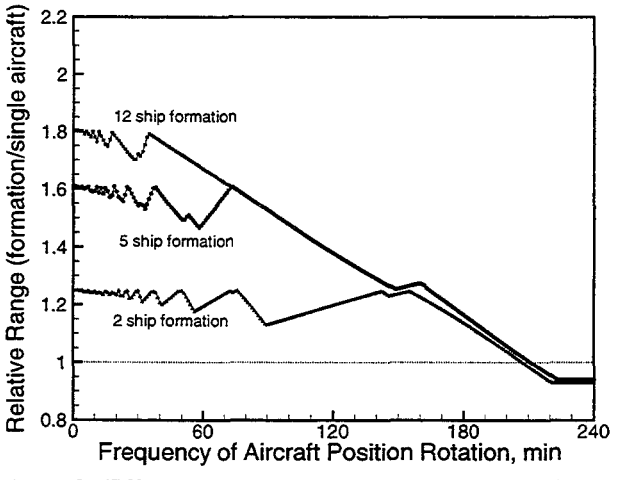

Figure 8. Effect of Rotation of Lead Aircraft on Relative Range. (M=0.85, 0.05 span position accuracy)

Formation Size

The effect of formation size on relative range is shown in Fig. 9. Also shown is the propulsion limit for a cruise/idle fuel flow ratio of one third, typical for low bypass engines at this flight condition. For this calculation, lateral position was assumed to be maintained within 0.05 span, with the lead aircraft rotating at ten minute intervals. As more aircraft are added, relative range increases up to a maximum of about 1.8. As formation size in increased beyond five or six aircraft, the additional payoff is rapidly diminished. For all formations larger than two aircraft, the desired flight altitude could not be achieved due to the thrust required on the lead aircraft exceeding the thrust available. For the five aircraft formation, the desired initial cruise altitude was 53,900 ft, the maximum attainable cruise altitude was 48,450 ft. This raised an interesting question. Would relative range increase if the lead aircraft used afterburner to increase its attainable cruise altitude?. The answer is negative, as shown in the filled circles in Fig 9.

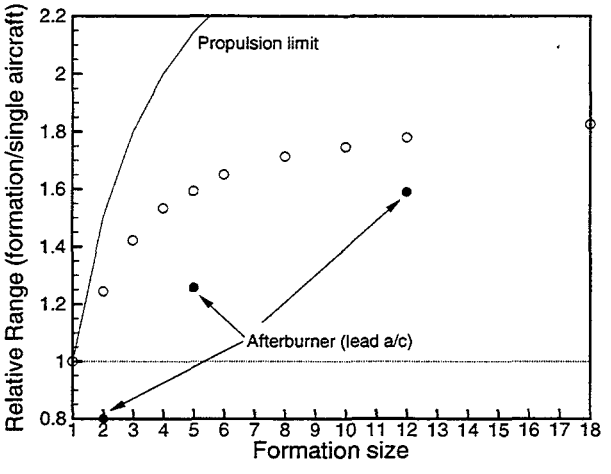

Figure 9. Effect of Formation Size on Relative Range. (M=0.85, 10 min rotation, 0.05 span position accuracy)

LATERAL-DIRECTIONAL STABILITY

Reductions in induced drag in formation flight are accompanied by changes in lift, side force, and moments about all three axes. The horseshoe model can be used to estimate the rolling and yawing moment increments induced on a trail wing, with the results obtained in the following form:

$$\Delta C_{l,k} = \frac{2C_{L,j}}{AR}\tau_{12} \qquad (22)$$

$$\Delta C_{n,k} = \frac{C_{L,j}C_{L,k}}{\pi AR}\tau_{12} \qquad (23)$$

Note that these relationships are for the wing only and do not include any vertical tail effects, which can be significant, especially in side force and yaw.

Contours of the influence factor τ_{12} are shown in Fig. 10. These values were obtained using the horseshoe vortex model with no core (μ=0). Large positive moments are found for aircraft spacings larger than the vortex separation ($\eta > \pi/4$) with negative moments

with small lateral spacings and/or large vertical spacings. For the conditions of high drag reduction ($\eta = \pi/4$), the trail aircraft has a tendency to roll and yaw away from its leader. The induced moments are stable with lateral position for $\eta > \pi/4$. A highly unstable region exists for $0.5 < \eta < \pi/4$.

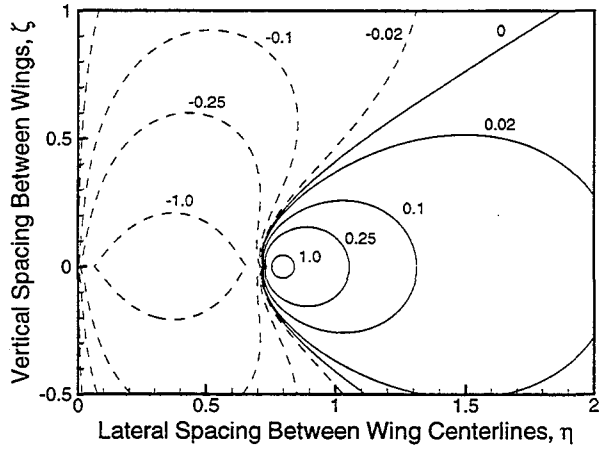

Figure 10. Variation in Rolling/Yawing Moment Factor τ_{12} With Aircraft Position, Horseshoe Vortex Model.

Fig. 11 compares horseshoe vortex predictions with and without a core with vortex lattice results from HASC95. These figures are directly analogous to the induced drag results of Figs. 2 and 4. The trend of the vortex lattice results is similar to the horseshoe results, with smaller peak values. As with the induced drag predictions, peak values for the vortex lattice results occur near wingtip spacing, as opposed to the $\pi/4$ spacing of the horseshoe results. The vortex lattice result also shows the unstable region, but with a smaller slope than the horseshoe result.

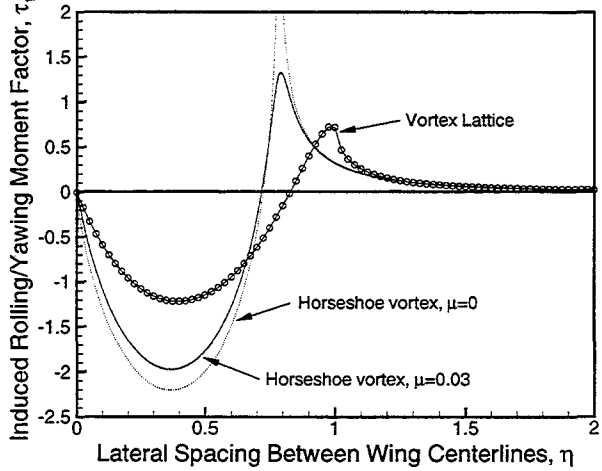

Figure 11. Rolling/Yawing Moment Predicted by Various Methods, ζ=0.

The above results are for a wing alone, different trends could result for a complete configuration. A formation flight analysis of two F-18's using HASC95 has been made which shows a larger yaw/roll moment ratio than the wing alone result and a negative side force. The side force and most of the increased yaw was due to suction forces on the vertical tails of the aft F-18. Wake induced rolling and yawing moments of the same sign mean a roll control device with proverse yaw would provide the best trim solution without excessive rudder deflection. Differential all moving tails typically exhibit proverse yaw at low angles of attack and also provide a side force in the proper direction. Use of these surfaces to trim the F-18 in roll and yaw resulted in a decrease in the induced drag benefit of one third on the trail aircraft. Maskew [7] has pointed out that roll trim using the proper wing control surface can further reduce the induced drag on the trail aircraft by making its wing lift distribution more elliptical. Conventional ailerons exhibit adverse yaw, however, which would require additional rudder for yaw and side force trim. A complete study of the various control surface options available is needed to determine the minimum "trim drag" condition.

The HASC95 F-18 results showed that the induced lift, pitching moment and rolling moment on the trail aircraft were effectively independent of the trail aircraft angle of attack (C_L) and were only functions of the relative aircraft spacing (Δx, Δy, Δz) and the lead aircraft angle of attack (C_L). The induced drag, side force and yawing moment were found to be functions of the trail aircraft angle of attack as well as the other variables. These findings are consistent with the horseshoe vortex results developed in the appendix, and suggest possible simplifications for developing aerodynamic math models for simulation.

CONCLUSION

Analysis of the induced drag effects of close formation flight has found:

a) Large reductions in induced drag are possible. These are accompanied by changes in lift, side force and moments about all three axes. Predictions of the magnitude of these changes using horseshoe vortex and vortex lattice methods give similar trends with differences in the predicted lateral position of maximum drag reduction.

b) The distribution of lift (aircraft weight) across a formation which maximizes drag reduction is elliptical, with the heavier aircraft in the center and lighter aircraft on the ends. This formation can be mimicked in operation by using a single echelon with the lead aircraft changing position to the rear on a periodic basis. This formation is also desirable from a safety standpoint.

c) The optimum cruise altitude of a formation is much higher than an equivalent single aircraft. The performance of the propulsion system at these conditions (ability to attain required thrust for cruise, decreased ratio of cruise thrust/idle thrust fuel flow, variations in specific fuel consumption) reduces the attainable range increase.

d) Simulations of the cruise leg of a constant Mach ferry mission show that range increases of sixty percent are possible for a five aircraft formation relative to a single aircraft. The ability to accurately maintain lateral position is critical. Fifty percent of the drag benefit is lost if the lateral/vertical position cannot be maintained to better than one tenth of a wing span.

e) Trim of the wake induced forces and moments may further reduce the drag benefit. Roll control devices that provide proverse yaw are desirable from this viewpoint.

ACKNOWLEDGMENTS

This work was conducted under a joint program of the Air Force Office of Scientific Research and the Air Force Research Laboratory. The authors would like to thank James Simon and Lex Parker for their assistance with the HASC95 analyses.

REFERENCES

1. Lissaman, P.B.S., and Shollenberger, C.A., "Formation Flight of Birds," Science, Vol. 168, pp. 1003-1005, 22 May 1970.

2. Hainsworth, F.R., "Precision and Dynamics or Positioning by Canada Geese Flying in Formation," Journal of Experimental Biology, Vol. 128, pp. 445-462, 1987.

3. Hoerner, S.F., "Fluid Dynamic Drag," published by the author, 1965.

4. Hummel, D., "Aerodynamic Aspects of Formation Flight in Birds," Journal of Theoretical Biology, Vol. 104, pp. 321-347, 1983.

5. Kshatriya, M., and Blake, R.W., "Theoretical Model of the Optimum Flock Size of Birds Flying in Formation," Journal of Theoretical Biology, Vol. 157, pp. 135-174, 1992.

6. Filippone, A., "Heuristic Optimization Applied to an Intrinsically Difficult Problem: Birds Formation Flight," AIAA paper 96-0515, January 1996.

7. Maskew, B., "Formation Flying Benefits Based on Vortex Lattice Calculations," NASA CR-151974, May 1977.

8. Beukenberg, M. and Hummel, D., "Aerodynamics, Performance and Control of Airplanes in Formation Flight," ICAS paper 90-5.9.3, 1990.

9. Prandtl, L., "Induced Drag of Multiplanes," NACA TN 182, March 1924.

10. Hallock, J.N., "Aircraft Wake Vortices: An Assessment of the Current Situation," DOT-FAA-RD-90-29, Jan 1991.

11. Albright, A.E., Dixon, C.J., and Hegedus, M.C., "Modification and Validation of Conceptual Design Aerodynamic Prediction Method HASC95 With VTXCHN," NASA CR-4712, March 1996.

12. Stewart, E.C., "A Study of the Interaction Between a Wake Vortex and an Encountering Airplane," AIAA-93-3642-CP, August 1993.

13. McKeehen, P.D., "GENESIS Simulation of a Modified VISTA F-16," AIAA-95-3381-CP, August 1995.

APPENDIX

The mutual induced drag factors σ_{jk} are derived here using the analysis of Hummel. Each wing's lift is represented as a single horseshoe vortex system, with the bound vortex at the wing quarter chord (Fig 1). If the wing lift is equivalent to that obtained from an elliptic load, the trailing vortex legs are separated by $(\pi/4)b$ and the vortex circulation strength is given by :

$$\Gamma = \frac{L}{\rho V b_v} = \frac{2Vb}{\pi AR} C_{L,j}$$

The lift vector of a wing section experiencing upwash from another wing is rotated forward by an amount equal to the upwash velocity divided by the freestream velocity (Fig A-1).

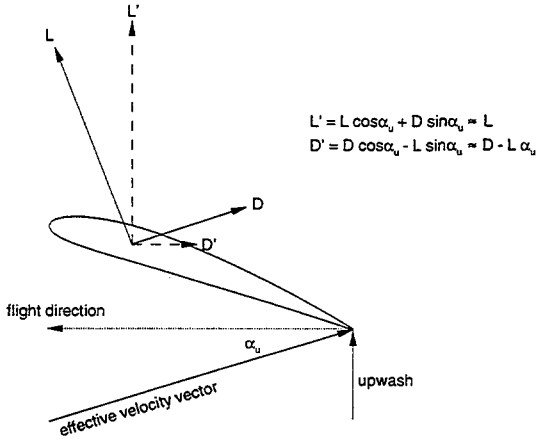

Figure A-1. Drag Reduction due to Upwash.

This reduces the induced drag of the wing rotation by an amount:

$$\Delta C_{Di,k} = -C_{L,k}\frac{w}{V}$$

The subscript j refers to the vortex generating wing while the subscript k refers to the wing for which the calculations are being made. The change in induced drag is obtained by integrating the upwash distribution across the lifting line of the wing:

$$\Delta C_{Di,k} = \frac{-C_{L,k}}{b_v}\int_{-b_v/2}^{b_v/2}\frac{w}{V}\,dy$$

The induced lift is given in a similar fashion as:

$$\Delta C_{L,k} = \frac{1}{b_v}\int_{-b_v/2}^{b_v/2} c_{l\alpha}\frac{w}{V}\,dy$$

The upwash w is proportional to the lift generated by the vortex generating wing. Two models for vortex induced velocity will be used. The first is the classical Helmholtz profile, which in conjunction with the Biot-Savart for a finite vortex gives:

$$V_\theta = \frac{\Gamma}{4\pi r}(\cos\delta_1 + \cos\delta_2)$$

The NASA Burnham profile gives:

$$V_\theta = \frac{\Gamma}{4\pi}\frac{r}{r^2 + r_c^2}(\cos\delta_1 + \cos\delta_2)$$

The integrals are now solved for several simplified cases.

Helmholtz profile with co-planar wings (ζ=0)

The upwash induced on the lifting line of the trail aircraft is obtained as:

$$\left(\frac{4\pi}{\Gamma_j}\right)w_k = \frac{1}{\Delta x}\left[\frac{y+\Delta y - b_v/2}{\sqrt{\Delta x^2 + (y+\Delta y - b_v/2)^2}} - \frac{y+\Delta y + b_v/2}{\sqrt{\Delta x^2 + (y+\Delta y + b_v/2)^2}}\right] + \frac{1}{y+\Delta y - b_v/2}\left(1 + \frac{\Delta x}{\sqrt{\Delta x^2 + (y+\Delta y - b_v/2)^2}}\right) - \frac{1}{y+\Delta y + b_v/2}\left(1 + \frac{\Delta x}{\sqrt{\Delta x^2 + (y+\Delta y + b_v/2)^2}}\right)$$

If wing k is upstream of wing j, a negative value is used for Δx. Evaluation of the integrals gives:

$$\Delta C_{Di,k} = \frac{C_{L,j}C_{L,k}}{\pi AR}\sigma_{jk}$$

$$\Delta C_{L,k} = \frac{-2C_{L,j}}{AR}\sigma_{jk}$$

with:

$$\left(\frac{\pi^2}{2}\right)\sigma_{jk} = \ln\left[1 - \left(\frac{\pi/4}{\eta}\right)^2\right]^2 - \frac{2\sqrt{\xi^2+\eta^2} - \sqrt{\xi^2 + (\eta - \pi/4)^2} - \sqrt{\xi^2 + (\eta + \pi/4)^2}}{\xi} - \ln\left[\frac{\left(\xi + \sqrt{\xi^2 + (\eta - \pi/4)^2}\right)\left(\xi + \sqrt{\xi^2 + (\eta + \pi/4)^2}\right)}{\left(\xi + \sqrt{\xi^2 + \eta^2}\right)^2}\right]$$

The spacing terms have been non-dimensionalized by the wing span. The mutual induced drag between any two aircraft is determined from the sum $\sigma_{jk}+\sigma_{kj}$. By definition:

$$\sigma_{jk}(\xi,\eta)=\sigma_{kj}(-\xi,-\eta)$$

This gives a greatly simplified result for the mutual effect:

$$\sigma_i \equiv \frac{\sigma_{jk}+\sigma_{kj}}{2}=\frac{1}{\pi^2}\ln\left[1-\left(\frac{\pi/4}{\eta}\right)^2\right]^2$$

This shows that the mutual induced drag is a function of the lateral spacing only, and is independent of longitudinal spacing, which is Munk's stagger theorem.

Helmholtz profile with infinitely spaced wings

Munk's theorem can be used to obtain the mutual induced drag of a two wing system by assuming the wings are infinitely spaced, so only the trailing vortices of the lead wing need be considered. The upwash is:

$$\left(\frac{2\pi}{\Gamma_j}\right)w_k=\frac{y+\Delta y-b_v/2}{z^2+(y+\Delta y-b_v/2)^2}-\frac{y+\Delta y+b_v/2}{z^2+(y+\Delta y+b_v/2)^2}$$

Giving:

$$\sigma_i=\frac{1}{\pi^2}\ln\left[\frac{\zeta^4+2\zeta^2\left(\eta^2+(\frac{\pi}{4})^2\right)+\left(\eta^2-(\frac{\pi}{4})^2\right)^2}{\left(\zeta^2+\eta^2\right)^2}\right]$$

Burnham profile with infinitely spaced wings

Repeating the analysis using the Burnham velocity profile gives:

$$\left(\frac{2\pi}{\Gamma_j}\right)w_k=\frac{y+\Delta y-b_v/2}{z^2+(y+\Delta y-b_v/2)^2+r_c^2}-\frac{y+\Delta y+b_v/2}{z^2+(y+\Delta y+b_v/2)^2+r_c^2}$$

And:

$$\sigma_i=\frac{1}{\pi^2}\ln\left[\frac{\zeta^2+\mu^2+(\eta-\pi/4)^2}{\zeta^2+\mu^2+\eta^2}\right]+\frac{1}{\pi^2}\ln\left[\frac{\zeta^2+\mu^2+(\eta+\pi/4)^2}{\zeta^2+\mu^2+\eta^2}\right]$$

Induced rolling and yawing moments on the trail aircraft can be found in a similar fashion:

$$\Delta C_{l,k}=\frac{-1}{bb_v}\int_{-b_v/2}^{b_v/2}c_{l\alpha}\frac{w}{V}y\,dy=\frac{2C_{L,j}}{AR}\tau_{12}$$

$$\Delta C_{n,k}=\frac{-C_{L,k}}{bb_v}\int_{-b_v/2}^{b_v/2}\frac{w}{V}y\,dy=\frac{C_{L,j}C_{L,k}}{\pi AR}\tau_{12}$$

For this case:

$$\tau_{jk}=\frac{2}{\pi^2}\ln\left[\frac{\mu^2+2\mu\left(\eta^2+(\frac{\pi}{4})^2\right)+\left(\eta^2-(\frac{\pi}{4})^2\right)^2}{\left(\mu^2+\eta^2\right)^2}\right]-\frac{1}{4\pi}\ln\left[\frac{\mu^2+\left(\eta+(\frac{\pi}{4})\right)^2}{\mu^2+\left(\eta-(\frac{\pi}{4})\right)^2}\right]$$